Highly Stable, Dual-Gated MoS_2 Transistors Encapsulated by Hexagonal Boron Nitride with Gate-Controllable Contact, Resistance, and Threshold Voltage

Gwan-Hyoung Lee,*,†,¶ Xu Cui,‡,¶ Young Duck Kim,‡ Ghidewon Arefe,‡ Xian Zhang,‡ Chul-Ho Lee,§ Fan Ye,∥ Kenji Watanabe,⊥ Takashi Taniguchi,⊥ Philip Kim,# and James Hone*,‡

†Department of Materials Science and Engineering, Yonsei University, Seoul 120-749, Korea, ‡Department of Mechanical Engineering and ∥Department of Material Science and Engineering, Columbia University, New York, New York 10027, United States, §KU-KIST Graduate School of Converging Science and Technology, Korea University, Seoul 136-701, Korea, ⊥National Institute for Materials Science, 1-1 Namiki, Tsukuba 305-0044, Japan, and #Department of Physics and Applied Physics, Harvard University, Cambridge, Massachusetts 02139, United States. ¶G.-H. Lee and X. Cui contributed equally.

ABSTRACT

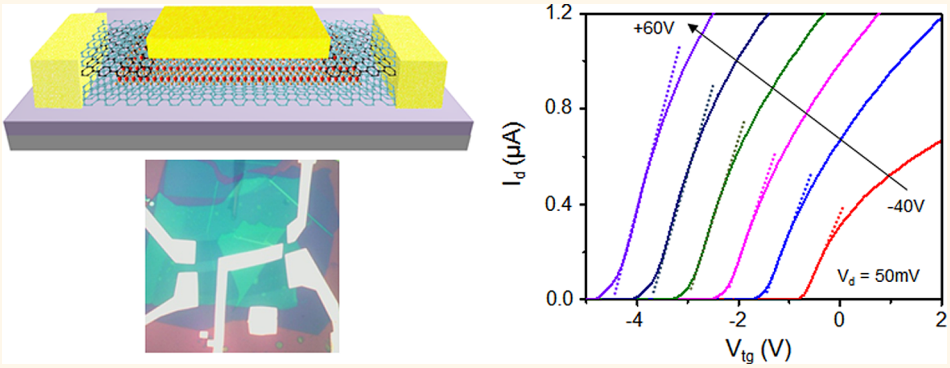

Emerging two-dimensional (2D) semiconductors such as molybdenum disulfide (MoS_2) have been intensively studied because of their novel properties for advanced electronics and optoelectronics. However, 2D materials are by nature sensitive to environmental influences, such as temperature, humidity, adsorbates, and trapped charges in neighboring dielectrics. Therefore, it is crucial to develop device architectures that provide both high performance and long-term stability. Here we report high performance of dual-gated van der Waals (vdW) heterostructure devices in which MoS_2 layers are fully encapsulated by hexagonal boron nitride (hBN) and contacts are formed using graphene. The hBN-encapsulation provides excellent protection from environmental factors, resulting in highly stable device performance, even at elevated temperatures. Our measurements also reveal high-quality electrical contacts and reduced hysteresis, leading to high two-terminal carrier mobility (33−151 $cm^2 V^{-1} s^{-1}$) and low subthreshold swing (80 mV/dec) at room temperature. Furthermore, adjustment of graphene Fermi level and use of dual gates enable us to separately control contact resistance and threshold voltage. This novel vdW heterostructure device opens up a new way toward fabrication of stable, high-performance devices based on 2D materials.

KEYWORDS: two-dimensional materials · MoS_2 · hexagonal boron nitride · graphene · van der Waals heterostructure · contact resistance · threshold voltage

Advances in graphene research have led to extensive interest in the unique electrical and optical properties of other 2D materials, in particular transition metal dichalcogenides (TMDCs).[1−5] Of these, semiconducting MoS_2 has been the most widely studied, showing a thickness-dependent electronic band structure[6,7] and high carrier mobility,[4,5,8−11] with applications in transistors,[4,8,12] memories,[13] logic circuits,[14] light-emitters,[2] and photodetectors[15] with flexibility and transparency.[1,3,5,16] However, as for any atomically thin material, the performance of MoS_2 devices can be strongly altered by environmental effects such as adsorbates, charges in neighboring dielectrics, and variability of contact quality.[5,17,18] For example, the measured mobilities of

* Address correspondence to gwanlee@yonsei.ac.kr, jh2228@columbia.edu.

Received for review March 2, 2015 and accepted June 17, 2015.

Published online June 17, 2015
10.1021/acsnano.5b01341

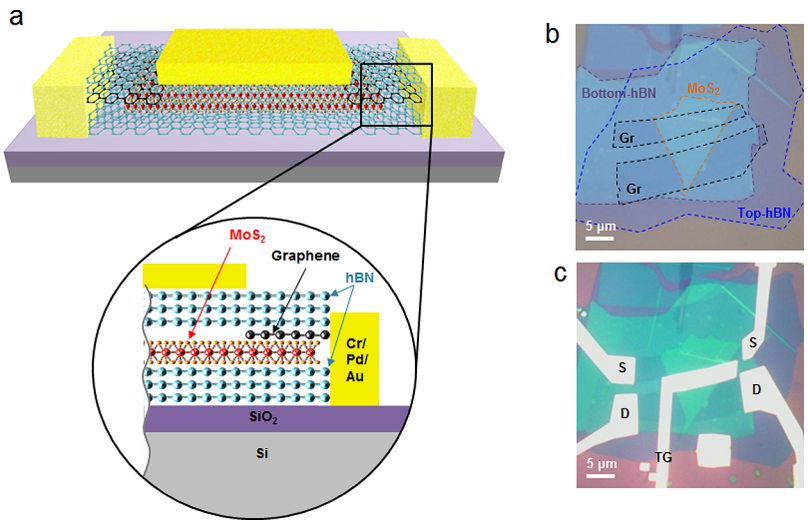

Figure 1. (a) Schematic of hBN-encapsulated MoS_2 field-effect transistor contacted with graphene electrodes. The enlarged schematic shows a cross-section of the contact area, where graphene is contacted along its edge with metal. Optical micrographs of (b) a stack of hBN/Gr/MoS_2/hBN before device fabrication and (c) the fabricated device. Dashed lines indicate boundaries of each 2D flake. Graphene was edge-contacted by metal leads of the source (S) and drain (D), and the top-gate (TG) was fabricated in the MoS_2 channel region.

MoS_2 at both room and low temperatures have been found to be substantially below theoretically predicted intrinsic values, which have been attributed to scattering of carriers by substrate roughness, charged impurities, substrate phonons, adsorbates on the surface, and electron−phonon coupling.[4,5,8,10,11,18−26] In addition, large contact resistance induced by the Schottky barrier at the metal−MoS_2 interface leads to low values of two-terminal field-effect mobility in MoS_2 devices.[9,16,27,28] More importantly, performance of MoS_2 field-effect transistors (FETs), whether exposed to air or passivated by conventional dielectrics such as HfO_2, is seen to substantially degrade over time[4,17,30] and create substantial sulfur vacancies during aggressive annealing, leading to heavily doped MoS_2 devices.[30] Therefore, the structural stability of MoS_2 cannot be neglected for maintaining performance of MoS_2 devices, and improvements in devices are required to eliminate environmental influences. For practical application of MoS_2 transistors, controllability of threshold voltage and low subthreshold swing are also desired.

Here we demonstrate vdW heterostructure MoS_2 devices with graphene contacts and dual gates, where the MoS_2 layer is entirely encapsulated by two hBN layers. We find that MoS_2 exposed to air or moisture experiences gradual degradation in electrical and optical properties, while the hBN-encapsulated MoS_2 is highly stable even at high temperature and shows no degradation for at least 8 months in ambient conditions. As a result, MoS_2 devices fabricated in this way show good two-terminal transport behavior indicative of high-quality contacts and high device stability, leading to high field-effect mobilities of 33−151 $cm^2\ V^{-1}\ s^{-1}$ at room temperature depending on MoS_2 thickness. By employing a dual-gate structure, we can achieve low operating voltage and independently modulate the graphene−MoS_2 contact resistance, the MoS_2 channel, and the threshold voltage. Our novel device scheme and fabrication technique show a new way toward investigation of the intrinsic properties of all other environmentally sensitive 2D materials and high-performance 2D material devices with long-term environmental stability.

RESULTS AND DISCUSSION

To fabricate the vdW heterostructures, we employed two polymer-free assembly techniques described in our previous reports.[5,31] In the first method, the top hBN flake is used to pick up other thin flakes by van der Waals adhesion to create a single stack that is then shaped into a device. In the second method, a stamp of PDMS (polydimethylsiloxane) elastomer is used to stack flakes one at a time to build the stack from the bottom up. Both techniques enable fabrication of ultraclean vdW interfaces without contamination of interfaces by polymer or solvent, which can leave residue and trapped bubbles[32] (see Methods and Supporting Information for more details, Figure S1). Figure 1a shows a schematic of device structure of MoS_2 FETs fabricated in this work. Graphene is placed slightly overlapping the MoS_2 over a few micrometers to form an electrical contact. For encapsulation of MoS_2, two hBN flakes are positioned on top and bottom. The entire stack of 2D materials is then shaped to expose the edges of graphene by e-beam lithography and plasma etching, and metal leads are formed by metal deposition to contact the exposed graphene edges. For dual-gating, we fabricated a metal top-gate covering only the MoS_2 channel area. Figure 1b shows an optical micrograph of a representative two-terminal

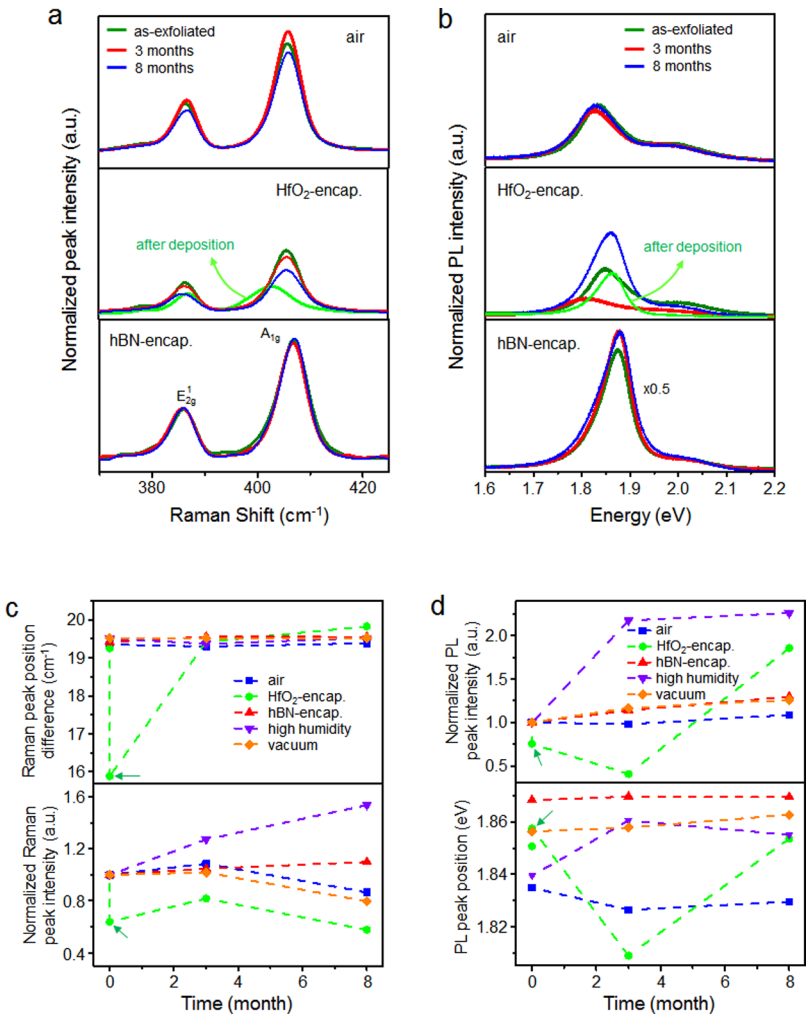

Figure 2. (a) Raman and (b) photoluminescence (PL) spectra of monolayer MoS_2 stored in different conditions. Among them, two MoS_2 flakes are encapsulated by HfO_2 and hBN, respectively, and then stored under ambient conditions. Compared to other samples, hBN-encapsulated MoS_2 shows no recognizable change in Raman and PL spectra. It should be noted that hBN-encapsulated MoS_2 also shows higher PL intensity due to the reduced effect of charged impurities from the substrate. (c) Raman peak position differences between E^1_{2g} and A_{1g} and Raman peak intensities of E^1_{2g} and (d) normalized PL peak intensities and PL peak positions in the monolayer MoS_2 samples stored in different conditions. The green arrows in (c) and (d) indicate the changes in the Raman spectrum and PL peak of the HfO_2-encapsulated sample right after deposition of HfO_2.

device, which is a stack of hBN (8 nm)/graphene (5 layers)/MoS_2 (3 layers)/hBN (19 nm).

Environmental conditions, such as temperature, moisture, polymer residue, and physisorbed gases, critically affect the electrical and optical properties of 2D materials and their heterostructures.[4,17,24] Raman spectroscopy and photoluminescence (PL) measurement were employed to study the environmental stability of monolayer MoS_2 samples stored in various conditions, such as ambient air, high humidity, and vacuum at room temperature as shown in Figure 2. (See Supporting Information for detailed storage conditions and Figure S2 for humidity and vacuum samples.) As shown in Figure 2a and c, unencapsulated samples stored in air and under vacuum showed small decreases in peak intensities over a period of 8 months, with even larger changes seen in a humid environment. Samples encapsulated in HfO_2 showed a similar decrease, in addition to large changes upon deposition of the HfO_2 by atomic layer deposition. In contrast, the Raman spectrum of hBN-encapsulated MoS_2 stored in air remained unchanged for 8 months. The mechanisms for this degradation are not precisely known, but can result from doping by adsorbed molecules in air, while long-term storage in a vacuum can result in sulfur vacancies.[3,18,29] The abrupt change in the Raman spectrum right after deposition of HfO_2 indicates the possibility of chemical reaction between MoS_2 and chemicals used for atomic layer deposition (ALD). Figure 2b shows PL spectra of the same samples. The hBN-encapsulated MoS_2 shows brighter PL, with intensity over 3 times that of the unencapsulated samples on SiO_2, due to the absence of charged impurities. The sharp PL peak with a full width at half-maximum (fwhm) of 70 meV also indicates that hBN-encapsulated MoS_2 is in a cleaner electrostatic environment (Figure S2c).[33] The spectrum

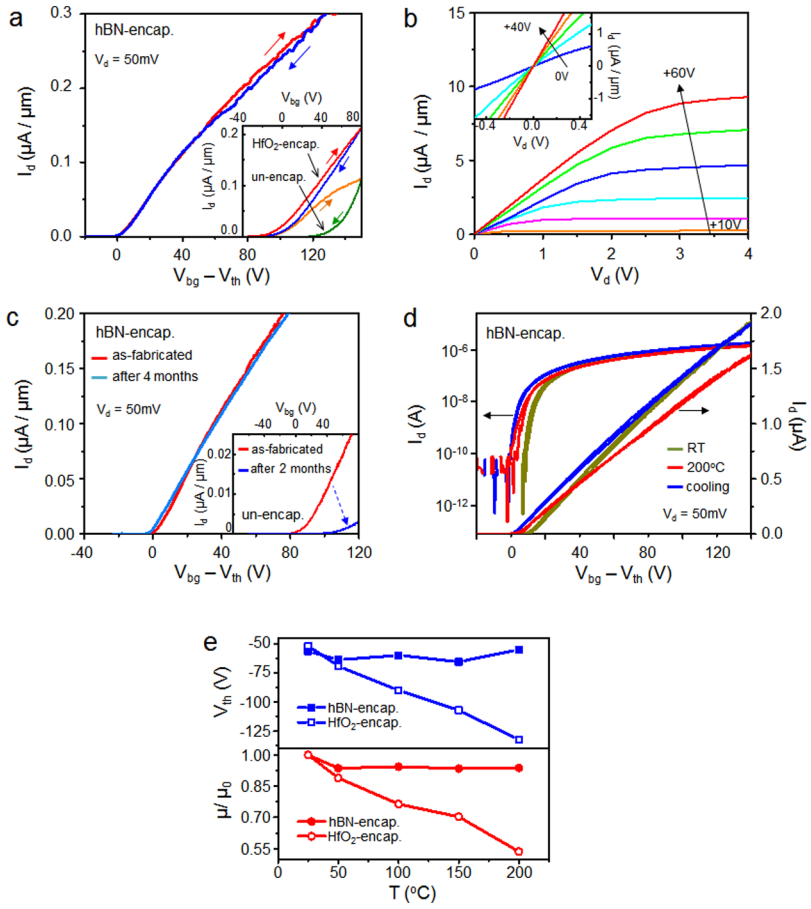

Figure 3. (a) Back-gated transfer curve (I_d−V_{bg}) of an hBN-encapsulated trilayer MoS_2 device, which shows a high two-terminal mobility of 69 cm^2/(V s) with no hysteresis. The inset, in comparison, shows the transfer curves of unencapsulated and HfO_2-encapsulated trilayer MoS_2 devices with a large hysteresis and low mobility of 7 cm^2/(V s) and 18 cm^2/(V s), respectively. (b) Output curves of a graphene-contacted MoS_2 device, varying the back-gate from +10 V to +60 V with steps of 10 V. The inset shows linear Ohmic graphene contact at small bias regime with varying back gate from 0 V to +40 V with steps of 10 V. (c) Transfer curve of the hBN-encapsulated trilayer MoS_2 device without degradation over 2 months, maintaining high performance. The inset shows the transfer curve of an unencapsulated trilayer MoS_2 device. After 2 months, it shows a dramatic decrease of mobility from 7 cm^2 V^{-1} s^{-1} to 1.2 cm^2 V^{-1} s^{-1}. (d) Transfer curves of the hBN-encapsulated trilayer MoS_2 device operating at different temperatures. When the device was heated from room temperature to 200 °C and then cooled, there is no performance degradation or change. (e) μ/μ_0, where μ_0 is mobility at room temperature, and threshold voltage (V_{th}) of HfO_2- and hBN-encapsulated trilayer MoS_2 devices when measured at increasing temperature.

shows virtually no change after 8 months of storage in air, as shown in Figure 2b and d. While the unencapsulated sample stored in air also shows little change in PL, HfO_2 encapsulation causes a complicated evolution of PL, indicative of strong interaction with the encapsulating layer. Changes of PL in the sample stored in humidity conditions and HfO_2-encapsulated conditions need more extensive experiments for interpretation even though it was reported that defect formation induces PL characteristics.[34,35]

To investigate the quality and stability of BN-encapsulated electronic devices, MoS_2 FETs were fabricated with no passivation or with HfO_2 or hBN encapsulation. Transfer curves (I_d−V_{bg}) for the vdW heterostructure device are shown in Figure 3a, with a back-gate voltage (V_{bg}) applied to the conductive Si back-gate with a 295 nm SiO_2 dielectric. The top-gate was grounded to avoid spurious dual-gate coupling.[36] The room-temperature field-effect mobility (μ_{FE}) of the two-terminal device was extracted by $\mu_{FE} = (L/(WC_iV_d))(dI_d/dV_{bg})$, where L, W, V_d, and V_{bg} are channel length, channel width, drain voltage, and back-gate voltage, respectively, and the capacitance per unit area (C_i) is $\varepsilon_0\varepsilon/d$, with relative permittivities of 3.9 and 3.5 for SiO_2 and hBN, respectively.[5] For the trilayer MoS_2 device of Figure 3a, the n-type two-terminal field-effect mobility is 69 cm^2 V^{-1} s^{-1}. The 12 hBN-encapsulated multilayer MoS_2 devices we tested in this work showed field-effect mobilities of 33−151 cm^2 V^{-1} s^{-1}, which are higher than previous reported values of 0.1−10 cm^2 V^{-1} s^{-1} in devices with metal contacts on oxide dielectrics[4,24,36−38] and comparable to the mobility recently reported with phase-engineered contacts (Table S1).[39] In addition, virtually no hysteresis is observed in hBN-encapsulated MoS_2 devices because of the charge-trap-free hBN dielectric and clean channel/dielectric interface.[5,13,22,40] By comparison, unencapsulated and HfO_2-encapsulated trilayer MoS_2 devices on SiO_2

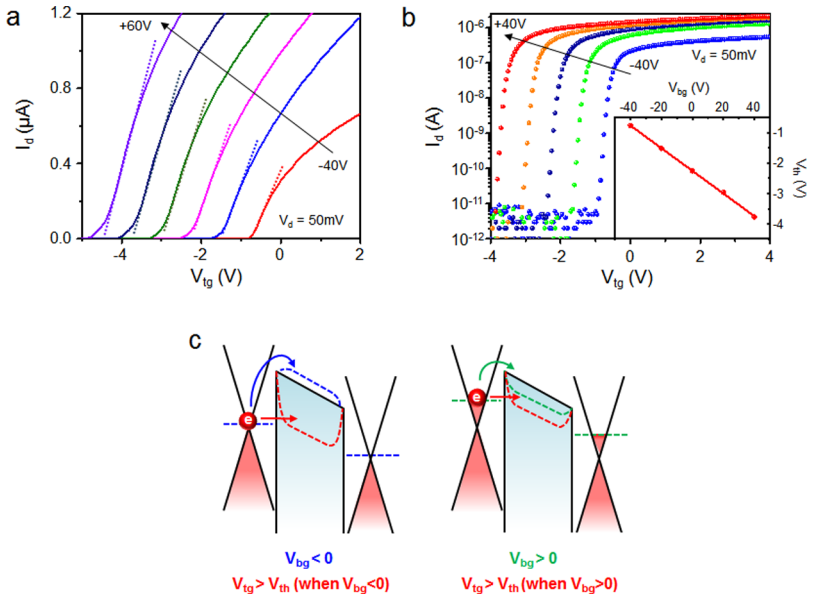

Figure 4. (a) Transfer curves of the top-gated hBN-encapsulated four-layer MoS_2 device with varying bottom-gate voltage. As the bottom-gate voltage increases from −40 V to +60 V, the field-effect mobility increases and the threshold voltage shifts to more positive top-gate voltage. The dashed lines indicate changes in the slope of dI_d/dV_{tg}. (b) Semilog scale transfer curves of (a) clearly show the shifts of threshold top-gate voltage. The inset shows the plots of top-gate threshold voltage (V_{th}) as a function of back-gate voltage (V_{bg}). The slope of the curve provides the capacitance ratio of the top and bottom dielectric. (c) Band diagrams of graphene-contacted MoS_2 in the vdW device at different bottom-gate voltages of $V_{bg} < 0$ (blue dashed line) and $V_{bg} > 0$ (green dashed line). When $V_{bg} > 0$, the Fermi level of graphene become close to the conduction band of MoS_2, resulting in a lowered contact barrier and highly positive top-gate threshold voltage.

with metal contacts showed lower mobilities of 7 and 18 $cm^2 V^{-1} s^{-1}$, respectively, and large hysteresis due to trapped charges and adsorbed impurities[13,24,29](Figure 3a, inset).

As shown in the inset of Figure 3b, the linear output curves (I_d−V_{ds}) of the hBN-encapsulated MoS_2 device reveal that Ohmic contacts are formed at graphene−MoS_2 interfaces. These high-quality contacts between graphene and MoS_2 have been attributed to the gate tunability of the graphene work function and the spatially narrow Schottky barrier in the ultrathin junction.[16,27,28,41,42] Gate modulation and current saturation are more clearly observed in Figure 3b. It should be noted that, even though it has been reported that Ohmic contacts have also been achieved in metal−MoS_2 contacts by deposition of small-work-function metal, vacuum annealing, and electrostatic gating,[10,11] conventional metal electrodes deposited on top of MoS_2 are not appropriate for these encapsulated devices, because of their finite thickness and the need for additional lithographic patterning, which leaves behind polymer residue on MoS_2 surface. Moreover, we did not observe any degradation or breakdown of the hBN-encapsulated MoS_2 devices up to high drain current of ~500 μA (6×10^7 A/cm^2), meaning that hBN-encapsulated MoS_2 devices can stably operate at higher current density than HfO_2-encapsulated MoS_2 devices with a breakdown current of 4.9×10^7 A/cm^2.[43]

Device stability is a critical issue for practical applications of 2D materials: moisture, atmospheric oxygen, physisorbed gases, and process-related polymer residue can strongly alter the electrical and optical properties of 2D materials and lead to degradation in performance over time.[4,17,24] For example, in unencapsulated trilayer MoS_2 FETs, the mobility degrades and the threshold voltage shifts after 2 months, as shown in the inset of Figure 3c, in good agreement with previous reports.[18,29] Encapsulation in conventional dielectrics such as HfO_2 and Al_2O_3 generally improves the mobility of MoS_2 FETs, but also causes large shifts of threshold voltage, and does not ensure long-term stability, as shown in the HfO_2-encapsulated trilayer MoS_2 device of Figure S3.[4] In contrast, Figure 3c shows that the hBN-encapsulated trilayer MoS_2 device experienced no electrical degradation after being stored in air for 4 months. (See Figures S4 and S5 for 1−6L MoS_2.) To explore the limits of this passivation, we investigated device stability at elevated temperatures. The hBN-encapsulated devices showed almost no change in performance after cycling to 200 °C and back to room temperature, as shown in Figure 3d and e. In contrast, unencapsulated mono- and bilayer devices were destroyed near 50 °C, while trilayer devices survived to 200 °C but showed large shifts in threshold voltage after cooling (Figures 3e and S6a and b). The HfO_2-encapsulated trilayer devices were able to withstand heating to 200 °C but showed a continuous decrease in mobility and large shift in threshold voltage with increasing temperature (Figures 3e and S6c). It is worth noting that there are kinks around zero gate voltage, called memory steps, in the transfer curve of the HfO_2-encapsulated MoS_2 device measured at 200 °C,

while none are observed in the hBN-encapsulated device (Figure S6c). The memory step results from the slow relaxation from capture/release of carriers by deep levels that are probably due to charged impurities in the substrate.[44,45] Therefore, the absence of memory steps in the hBN-encapsulated MoS_2 device strongly supports the cleanness of MoS_2−hBN heterointerfaces.

To control contact resistance and threshold voltage of dual-gated MoS_2 devices, we employed top- and bottom-gates simultaneously. Figure 4a shows transfer curves of a dual-gated four-layer MoS_2 device with sweeping top-gate voltage at fixed bottom-gate voltage. At V_{bg} = 0 V, the top-gated device exhibited a field-effect mobility of 37 $cm^2\ V^{-1}\ s^{-1}$, similar to 33 $cm^2\ V^{-1}\ s^{-1}$ measured in the same device tuned by the bottom-gate. With increasing V_{bg} from −40 V to +60 V, the mobility increases from 26 to 45 $cm^2\ V^{-1}\ s^{-1}$, and the threshold voltage shifts to more positive values. This threshold voltage shift was not seen in HfO_2-encapsulated MoS_2 devices with metal contacts.[4] As shown in Figure 4b, the dual-gated MoS_2 device shows a high on/off current ratio of 10^6 and a small subthreshold swing of 78−85 mV/dec, which means these devices can work at a small operation gate voltage of <1 V. The linear shift of the top-gate threshold voltage as a function of back-gate voltage is shown in the inset of Figure 4b. The slope of 0.0372 is in good agreement with the value predicted by the ratio of back-gate to top-gate capacitance. Schematic band diagrams of Figure 4c show bending of band structure in graphene-contacted MoS_2 at different back-gate voltages. When $V_{bg} < 0$, the graphene Fermi level shifts downward, creating a higher barrier, leading to a larger contact resistance and more negative top-gate threshold voltage. Conversely, when $V_{bg} > 0$, the Fermi level of graphene approaches the conduction band of MoS_2, creating a lower contact barrier, leading to lower contact resistance and more positive top-gate threshold voltage. The decreasing contact resistance causes an increase in the two-terminal field-effect mobility. Therefore, we can conclude that the vdW heterostructure device proposed in this study, hBN-encapsulated MoS_2 FETs with graphene electrodes, enables us to fabricate high-performance devices of environmentally sensitive 2D materials with high stability.

CONCLUSIONS

We demonstrate fabrication of hBN-encapsulated MoS_2 FETs contacted by graphene electrodes. These vdW heterostructure devices fulfill requirements for current electronics, such as low contact resistance, low operating gate voltage, tunable threshold voltage, high-temperature operation, lack of hysteresis, and stability over many months in ambient conditions. Similar heterostructure approaches have recently shown promise for providing environmental stability for more environmentally sensitive 2D materials such as phosphorene.[46,47] The results presented here indicate that hBN encapsulation can provide such stability over long time periods and at high temperatures required for practical device operation in applications.

METHODS

All the 2D materials are mechanically exfoliated by Scotch tape and then transferred by "van der Waals transfer" or "PDMS transfer" technique as described before.[5,33] The transfer techniques are described in detail in the Supporting Information. The hBN/Gr/MoS_2/hBN stacks were fabricated by transferring each flake on the SiO_2 substrate. After stacking 2D materials, metal leads were patterned by e-beam lithography, and graphene edges were exposed by etching the whole stack with inductively coupled plasma with a mixture of CHF_3 and O_2 gases. After exposure of graphene edges, metals of Cr 1 nm/Pd 20 nm/Au 50 nm were deposited by an e-beam evaporator. For the top-gate, an additional e-beam lithography process was performed. Raman spectroscopy (inVia, Renishaw) was employed to measure the Raman spectra and photoluminescence of single-layer MoS_2 flakes using a 532 nm laser. The different samples are stored in various conditions. The storing conditions are described in detail in the Supporting Information. The HfO_2- and hBN-encapsulated MoS_2 samples were stored in air. Here 30 nm thick HfO_2 was deposited by ALD. All the electrical measurements are performed in air at room temperature using a parameter analyzer (Agilent, 4155C).

Conflict of Interest: The authors declare no competing financial interest.

Acknowledgment. This research was supported by the U.S. National Science Foundation (DMR-1122594) and the NSF MRSEC program through Columbia in the Center for Precision Assembly of Superstratic and Superatomic Solids (DMR-1420634). G.H.L. acknowledges support from the Basic Science Research Program (NRF-2014R1A1A1004632) through the National Research Foundation (NRF) funded by the Korean government Ministry of Science, ICT and Future, and in part by the Yonsei University Future-Leading Research Initiative of 2014. C.H.L. acknowledges support from the Basic Science Research Program (NRF-2014R1A1A2055112) through the National Research Foundation (NRF) funded by the Korean government Ministry of Education, and in part from the Grant of KU-KIST Graduate School of Converging Science and Technology.

Supporting Information Available: The Supporting Information is available free of charge on the ACS Publications website at DOI: 10.1021/acsnano.5b01341.

REFERENCES AND NOTES

1. Wang, Q. H.; Kalantar-Zadeh, K.; Kis, A.; Coleman, J. N.; Strano, M. S. Electronics and Optoelectronics of Two-Dimensional Transition Metal Dichalcogenides. *Nat. Nanotechnol.* **2012**, *7*, 699–712.
2. Sundaram, R. S.; Engel, M.; Lombardo, A.; Krupke, R.; Ferrari, A. C.; Avouris, P.; Steiner, M. Electroluminescence in Single Layer MoS_2. *Nano Lett.* **2013**, *13*, 1416–1421.
3. Jariwala, D.; Sangwan, V. K.; Lauhon, L. J.; Marks, T. J.; Hersam, M. C. Emerging Device Applications for Semiconducting Two-Dimensional Transition Metal Dichalcogenides. *ACS Nano* **2014**, *8*, 1102–1120.
4. Radisavljevic, B.; Radenovic, A.; Brivio, J.; Giacometti, V.; Kis, A. Single-Layer MoS_2 Transistors. *Nat. Nanotechnol.* **2011**, *6*, 147–150.

5. Lee, G. H.; Yu, Y. J.; Cui, X.; Petrone, N.; Lee, C. H.; Choi, M. S.; Lee, D. Y.; Lee, C.; Yoo, W. J.; Watanabe, K.; *et al*. Flexible and Transparent MoS_2 Field-Effect Transistors on Hexagonal Boron Nitride-Graphene Heterostructures. *ACS Nano* **2013**, *7*, 7931–7936.
6. Mak, K. F.; Lee, C.; Hone, J.; Shan, J.; Heinz, T. F. Atomically Thin MoS_2: A New Direct-Gap Semiconductor. *Phys. Rev. Lett.* **2010**, *105*, 136805.
7. Lee, C.; Yan, H.; Brus, L. E.; Heinz, T. F.; Hone, J.; Ryu, S. Anomalous Lattice Vibrations of Single- and Few-Layer MoS_2. *ACS Nano* **2010**, *4*, 2695–2700.
8. Kim, S.; Konar, A.; Hwang, W. S.; Lee, J. H.; Lee, J.; Yang, J.; Jung, C.; Kim, H.; Yoo, J. B.; Choi, J. Y.; *et al*. High-Mobility and Low-Power Thin-Film Transistors Based on Multilayer MoS_2 Crystals. *Nat. Commun.* **2012**, *3*, 1011.
9. Das, S.; Chen, H. Y.; Penumatcha, A. V.; Appenzeller, J. High Performance Multilayer MoS_2 Transistors with Scandium Contacts. *Nano Lett.* **2012**, *13*, 100–105.
10. Radisavljevic, B.; Kis, A. Mobility Engineering and a Metal-Insulator Transition in Monolayer MoS_2. *Nat. Mater.* **2013**, *12*, 815–820.
11. Baugher, B. W. H.; Churchill, H. O. H.; Yang, Y. F.; Jarillo-Herrero, P. Intrinsic Electronic Transport Properties of High-Quality Monolayer and Bilayer MoS_2. *Nano Lett.* **2013**, *13*, 4212–4216.
12. Britnell, L.; Gorbachev, R. V.; Jalil, R.; Belle, B. D.; Schedin, F.; Mishchenko, A.; Georgiou, T.; Katsnelson, M. I.; Eaves, L.; Morozov, S. V.; *et al*. Field-Effect Tunneling Transistor Based on Vertical Graphene Heterostructures. *Science* **2012**, *335*, 947–950.
13. Choi, M. S.; Lee, G. H.; Yu, Y. J.; Lee, D. Y.; Lee, S. H.; Kim, P.; Hone, J.; Yoo, W. J. Controlled Charge Trapping by Molybdenum Disulphide and Graphene in Ultrathin Heterostructured Memory Devices. *Nat. Commun.* **2013**, *4*, 1624.
14. Wang, H.; Yu, L. L.; Lee, Y. H.; Shi, Y. M.; Hsu, A.; Chin, M. L.; Li, L. J.; Dubey, M.; Kong, J.; Palacios, T. Integrated Circuits Based on Bilayer MoS_2 Transistors. *Nano Lett.* **2012**, *12*, 4674–4680.
15. Britnell, L.; Ribeiro, R. M.; Eckmann, A.; Jalil, R.; Belle, B. D.; Mishchenko, A.; Kim, Y.-J.; Gorbachev, R. V.; Georgiou, T.; Morozov, S. V.; *et al*. Strong Light-Matter Interactions in Heterostructures of Atomically Thin Films. *Science* **2013**, *340*, 1311–1314.
16. Yoon, J.; Park, W.; Bae, G. Y.; Kim, Y.; Jang, H. S.; Hyun, Y.; Lim, S. K.; Kahng, Y. H.; Hong, W. K.; Lee, B. H.; *et al*. Highly Flexible and Transparent Multilayer MoS_2 Transistors with Graphene Electrodes. *Small* **2013**, *9*, 3295–3300.
17. Tongay, S.; Zhou, J.; Ataca, C.; Liu, J.; Kang, J. S.; Matthews, T. S.; You, L.; Li, J. B.; Grossman, J. C.; Wu, J. Q. Broad-Range Modulation of Light Emission in Two-Dimensional Semiconductors by Molecular Physisorption Gating. *Nano Lett.* **2013**, *13*, 2831–2836.
18. Qiu, H.; Pan, L. J.; Yao, Z. N.; Li, J. J.; Shi, Y.; Wang, X. R. Electrical Characterization of Back-Gated Bi-Layer MoS_2 Field-Effect Transistors and the Effect of Ambient on Their Performances. *Appl. Phys. Lett.* **2012**, *100*, 123104.
19. Kaasbjerg, K.; Thygesen, K. S.; Jacobsen, K. W. Phonon-Limited Mobility in n-Type Single-Layer MoS_2 from First Principles. *Phys. Rev. B* **2012**, *85*, 115317.
20. Li, X. D.; Mullen, J. T.; Jin, Z. H.; Borysenko, K. M.; Nardelli, M. B.; Kim, K. W. Intrinsic Electrical Transport Properties of Monolayer Silicene and MoS_2 from First Principles. *Phys. Rev. B* **2013**, *87*, 115418.
21. Ma, N.; Jena, D. Charge Scattering and Mobility in Atomically Thin Semiconductors. *Phys. Rev. X* **2014**, *4*, 011043.
22. Dean, C. R.; Young, A. F.; Meric, I.; Lee, C.; Wang, L.; Sorgenfrei, S.; Watanabe, K.; Taniguchi, T.; Kim, P.; Shepard, K. L.; *et al*. Boron Nitride Substrates for High-Quality Graphene Electronics. *Nat. Nanotechnol.* **2010**, *5*, 722–726.
23. Kaasbjerg, K.; Thygesen, K. S.; Jauho, A. P. Acoustic Phonon Limited Mobility in Two-Dimensional Semiconductors: Deformation Potential and Piezoelectric Scattering in Monolayer MoS_2 from First Principles. *Phys. Rev. B* **2013**, *87*, 235312.
24. Bao, W. Z.; Cai, X. H.; Kim, D.; Sridhara, K.; Fuhrer, M. S. High Mobility Ambipolar MoS_2 Field-Effect Transistors: Substrate and Dielectric Effects. *Appl. Phys. Lett.* **2013**, *102*, 042104.
25. Ghatak, S.; Pal, A. N.; Ghosh, A. Nature of Electronic States in Atomically Thin MoS_2 Field-Effect Transistors. *ACS Nano* **2011**, *5*, 7707–7712.
26. Cui, X.; Lee, G. H.; Kim, Y. D.; Arefe, G.; Huang, P. Y.; Lee, C. H.; Chenet, D. A.; Zhang, X.; Wang, L.; Ye, F.; *et al*. Multi-Terminal Transport Measurements of MoS_2 Using a van der Waals Heterostructure Device Platform. *Nat. Nanotechnol.* **2015**, *10*, 534–540.
27. Liu, H.; Neal, A. T.; Ye, P. D. Channel Length Scaling of MoS_2 MOSFETs. *ACS Nano* **2012**, *6*, 8563–8569.
28. Lee, Y. T.; Choi, K.; Lee, H. S.; Min, S. W.; Jeon, P. J.; Hwang, D. K.; Choi, H. J.; Im, S. Graphene *versus* Ohmic Metal as Source-Drain Electrode for Mo_S Nanosheet Transistor Channel. *Small* **2014**, *10*, 2356–2361.
29. Late, D. J.; Liu, B.; Matte, H. S. S. R.; Dravid, V. P.; Rao, C. N. R. Hysteresis in Single-Layer MoS_2 Field Effect Transistors. *ACS Nano* **2012**, *6*, 5635–5641.
30. Zhou, W.; Zou, X.; Najmaei, S.; Liu, Z.; Shi, Y.; Kong, J.; Lou, J.; Ajayan, P. M.; Yakobson, B. I.; Idrobo, J. C. Intrinsic Structural Defects in Monolayer Molybdenum Disulfide. *Nano Lett.* **2013**, *13*, 2615–22.
31. Wang, L.; Meric, I.; Huang, P. Y.; Gao, Q.; Gao, Y.; Tran, H.; Taniguchi, T.; Watanabe, K.; Campos, L. M.; Muller, D. A.; *et al*. One-Dimensional Electrical Contact to a Two-Dimensional Material. *Science* **2013**, *342*, 614–617.
32. Haigh, S. J.; Gholinia, A.; Jalil, R.; Romani, S.; Britnell, L.; Elias, D. C.; Novoselov, K. S.; Ponomarenko, L. A.; Geim, A. K.; Gorbachev, R. Cross-Sectional Imaging of Individual Layers and Buried Interfaces of Graphene-Based Heterostructures and Superlattices. *Nat. Mater.* **2012**, *11*, 764–767.
33. van der Zande, A. M.; Huang, P. Y.; Chenet, D. A.; Berkelbach, T. C.; You, Y. M.; Lee, G. H.; Heinz, T. F.; Reichman, D. R.; Muller, D. A.; Hone, J. C. Grains and Grain Boundaries in Highly Crystalline Monolayer Molybdenum Disulphide. *Nat. Mater.* **2013**, *12*, 554–561.
34. Chow, P. K.; Jacobs-Gedrim, R. B.; Gao, J.; Lu, T.-M.; Yu, B.; Terrones, H.; Koratkar, N. Defect-Induced Photoluminescence in Monolayer Semiconducting Transition Metal Dichalcogenides. *ACS Nano* **2015**, *9*, 1520–1527.
35. Nan, H. Y.; Wang, Z. L.; Wang, W. H.; Liang, Z.; Lu, Y.; Chen, Q.; He, D. W.; Tan, P. H.; Miao, F.; Wang, X. R.; *et al*. Strong Photoluminescence Enhancement of MoS_2 through Defect Engineering and Oxygen Bonding. *ACS Nano* **2014**, *8*, 5738–5745.
36. Fuhrer, M. S.; Hone, J. Measurement of Mobility in Dual-Gated MoS_2 Transistors. *Nat. Nanotechnol.* **2013**, *8*, 146–147.
37. Novoselov, K. S.; Jiang, D.; Schedin, F.; Booth, T. J.; Khotkevich, V. V.; Morozov, S. V.; Geim, A. K. Two-Dimensional Atomic Crystals. *Proc. Natl. Acad. Sci. U.S.A.* **2005**, *102*, 10451–10453.
38. Ayari, A.; Cobas, E.; Ogundadegbe, O.; Fuhrer, M. S. Realization and Electrical Characterization of Ultrathin Crystals of Layered Transition-Metal Dichalcogenides. *J. Appl. Phys.* **2007**, *101*, 014507.
39. Kappera, R.; Voiry, D.; Yalcin, S. E.; Branch, B.; Gupta, G.; Mohite, A. D.; Chhowalla, M. Phase-Engineered Low-Resistance Contacts for Ultrathin MoS_2 Transistors. *Nat. Mater.* **2014**, *13*, 1128–1134.
40. Kang, S. J.; Lee, G. H.; Yu, Y. J.; Zhao, Y.; Kim, B.; Watanabe, K.; Taniguchi, T.; Hone, J.; Kim, P.; Nuckolls, C. Organic Field Effect Transistors Based on Graphene and Hexagonal Boron Nitride Heterostructures. *Adv. Funct. Mater.* **2014**, *24*, 5157–5163.
41. Du, Y. C.; Yang, L. M.; Zhang, J. Y.; Liu, H.; Majumdar, K.; Kirsch, P. D.; Ye, P. D. MoS_2 Field-Effect Transistors with Graphene/Metal Heterocontacts. *IEEE Electron Device Lett.* **2014**, *35*, 599–601.
42. Bertolazzi, S.; Krasnozhon, D.; Kis, A. Nonvolatile Memory Cells Based on MoS_2/Graphene Heterostructures. *ACS Nano* **2013**, *7*, 3246–3252.
43. Lembke, D.; Kis, A. Breakdown of High-Performance Monolayer MoS_2 Transistors. *ACS Nano* **2012**, *6*, 10070–10075.

44. Rumyantsev, S. L.; Liu, G. X.; Shur, M. S.; Balandin, A. A. Observation of the Memory Steps in Graphene at Elevated Temperatures. *Appl. Phys. Lett.* **2011**, *98*, 222107.
45. Kim, Y. D.; Bae, M. H.; Seo, J. T.; Kim, Y. S.; Kim, H.; Lee, J. H.; Ahn, J. R.; Lee, S. W.; Chun, S. H.; Park, Y. D. Focused-Laser-Enabled p-n Junctions in Graphene Field-Effect Transistors. *ACS Nano* **2013**, *7*, 5850–5857.
46. Cao, Y.; Mishchenko, A.; Yu, G. L.; Khestanova, K.; Rooney, A.; Prestat, E.; Kretinin, A. V.; Blake, P.; Shalom, M. B.; Balakrishnan, G.; *et al*. Quality Heterostructures from Two Dimensional Crystals Unstable in Air by Their Assembly in Inert Atmosphere. *arXiv:1502.03755*, **2015**.
47. Gillgren, N.; Wickramaratne, D.; Shi, Y.; Espiritu, T.; Yang, J.; Hu, J.; Wei, J.; Liu, X.; Mao, Z.; Watanabe, K. Gate Tunable Quantum Oscillations in Air-Stable and High Mobility Few-Layer Phosphorene Heterostructures. *2D Mater.* **2015**, *2*, 011001.